Geomechanics and Engineering, *Vol. 11, No. 5 (2016) 713-723*
DOI: http://dx.doi.org/10.12989/gae.2016.11.5.713

Shear wave velocity of sands subject to large strain triaxial loading

Supot Teachavorasinskun [*1] and Pulpong Pongvithayapanu [2a]

[1] Department of Civil Engineering, Faculty of Engineering,
Chulalongkorn University, Phayathai Road, Pathumwan, Bangkok, Thailand
[2] Department of Civil Engineering, Faculty of Engineering at Si Racha,
Kasetsart University, Chonburi, Thailand

(*Received December 06, 2015, Revised June 07, 2016, Accepted July 04, 2016*)

Abstract. Shear wave velocities of three selected sandy soils subject to drained triaxial compression test were continuously measured using the bender elements. The shear wave velocity during isotropic compression, as widely recognized, increased as confining pressure increased and they were correlated well. However, during drained shearing, the mean effective stress could no further provide a suitable correlation. The shear wave velocity during this stage was almost constant with respect to the mean effective stress. The vertical stress was found to be more favorable at this stage (since confining stress was kept constant). When sample was attained its peak stress, the shear wave velocity reduced and deviated from the previously existed trend line. This was probably caused by the non-uniformity induced by the formation of shear band. Subsequently, void ratios computed based on external measurements could not provide reasonable fitting to the initial stage of post-peak shear wave velocity. At very large strain levels after shear band formation, the digital images revealed that sample may internally re-arrange itself to be in a more uniform loose stage. This final stage void ratio estimated based on the proposed correlation derived during pre-peak state was close to the value of the maximum void ratio.

Keywords: shear wave velocity; shear band; triaxial compression test; sandy soil

1. Introduction

The characteristics of shear wave velocity of soils are highly dependent on the states of effective stresses, void ratio, grain characteristics and stress history (Iwasaki *et al*. 1978, Roesler 1979, Yu and Richart 1984, Stokoe *et al*. 1995, Bellotti *et al*. 1996, Teachavorasinskun *et al*. 2002, and Teachavorasinskun and Akkarakun 2004, Ku and Mayne 2015). Nevertheless, very limited number of literature actually employed those elastic stiffness characteristics in geotechnical analysis (Silvestri and Abou-Samra 2009 and Clayton 2011). It is conventionally and practically adopted in most geotechnical analyses, especially for the elasto-plastic computation, to determine the elastic properties of soils based solely on its initial stress states. No matter what stress states involve in later loading conditions, soils are assumed to maintain their elastic constants for sake of simplicity. This approximation eases engineers in conducting their analysis, though contradicting

---

∗Corresponding author, Associate Professor, E-mail: tsupot@chula.ac.th
[a] Ph.D., E-mail: srcpppn@ku.ac.th

http://www.techno-press.org/?journal=gae&subpage=7 ISSN: 2005-307X (Print), 2092-6219 (Online)

to the general recognized fact. Although plastic deformation may mainly influence the overall soil behavior at large strain level, soil elasticity still plays an important role by acting as the skeleton for plastic calculation. In most laboratory tests, differentiation between elastic and plastic deformations is difficult, except during soil undergoes unloading. It is therefore the aim of the present study to examine the existence of soil elasticity during large strain shearing by measuring the small strain shear wave velocity during triaxial compression.

Furthermore, after peak shear stress is attained, strain localization occurs and greatly affects soil's post peak behaviors. Strain localization has been well recognized to be dependent on the initial states of effective stresses, void ratios, grain characteristics and stress history (Desrues and Viggiani 2004, Higo *et al*. 2013). Since strain localization and velocity of shear wave propagation primarily depend on some common key factors, their relation may reasonably be expected similar to those drawn in liquefaction problem (Xu *et al.* 2015). Continuation of shear wave velocity measurement may probably provide a preliminary view of strain location.

2. Materials and testing method

The tested sand was taken from the eastern region of Thailand. Their grain particles were round to sub-angular shapes. This original sand was sieved to provide two batches of more uniform testing materials. The first batch (called herein D16 sand) was that with grain size being greater than 1.18 mm (sieve No. 16). The other (D40 sand) was a finer one having particles passing through sieve No. 16 but retaining on sieve No. 40 (sieve opening = 0.425 mm). The physical properties and particle shapes of those two sieved sands are summarized in Table 1 and Fig. 1. Sieving was done in order to provide a more uniform sand to increase possibility to observe

Table 1 Basic physical property of tested sands

Basic property	D16	D40	*Silica*
Shape of grain particle	Low to medium sphericity with angular shape	Low to medium sphericity with angular shape	High sphericity with well rounded shape
Mean size particle, d_{50} (mm)	1.18	0.465	0.60
Specific gravity, G_s	2.69	2.72	2.65
Maximum void ratio, e_{max}	1.06	1.12	0.6
Minimum void ratio, e_{min}	0.713	0.808	0.459

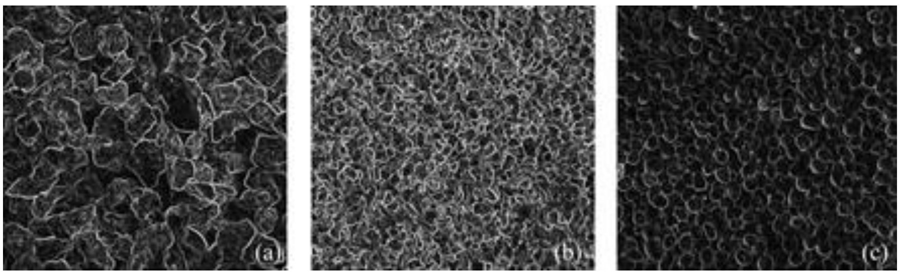

Fig. 1 Shapes of grain particles of (a) D16; (b) D40; and (c) *Silica* sands

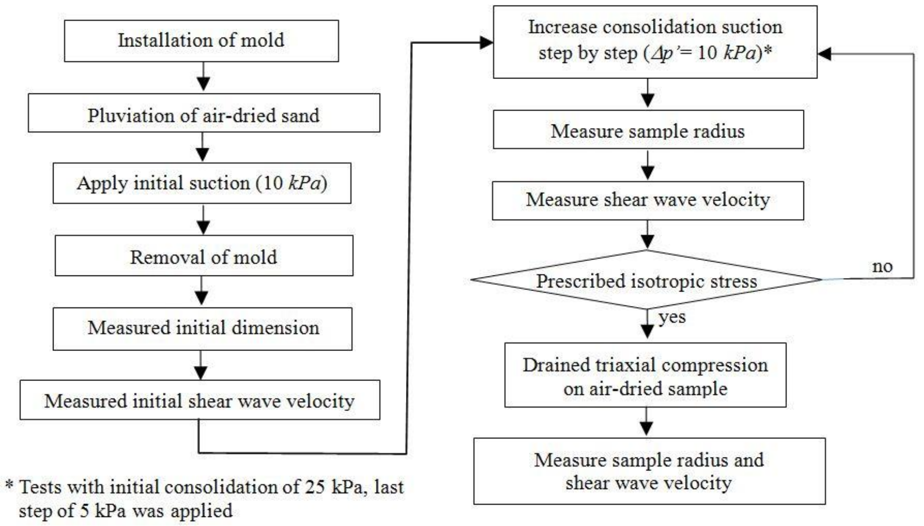

Fig. 2 Flow diagram depicting the testing procedure

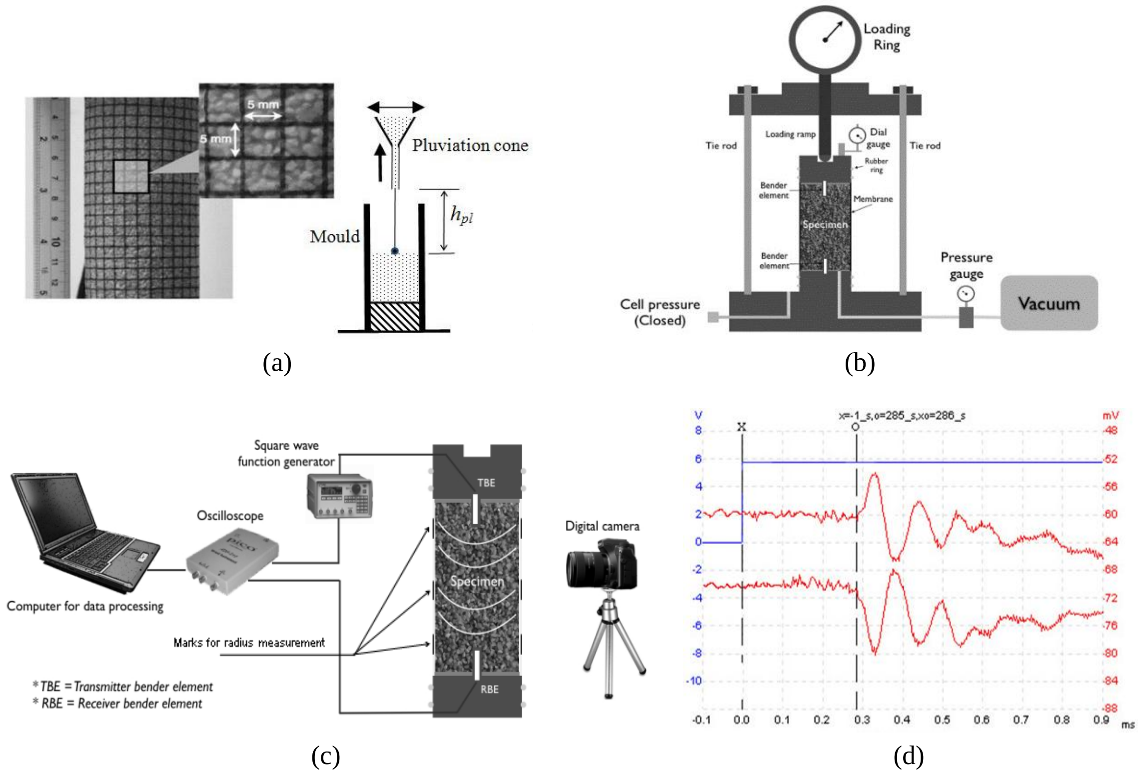

Fig. 3 General arrangement of equipment used in the study: (a) the square grid of 5×5 mm mounted on the outer surface of rubber membrane and pluviation method; (b) schematic view of triaxial equipment used in the study; (c) schematic view of the bender element setup; and (d) typical measured shear waves

localization. In addition, commercially available silica sand conformed to the ASTM C-778 #20 – 30 was also tested in this study.

The sample preparation and testing procedure are summarized in Fig. 2. A sample was prepared by air-pluviating air-dried sand from a specific height into a split mould having inner diameter and height of 5 and 10 cm. The small pluviation cone, filled with sand, was slowly moved horizontally and vertically so that the height of pluviation (from sample's surface) remained constant until the mould was full (Fig. 3(a)). Mould was assembled around the pedestal, where the bending element was pre-installed. A top cap, with top bender element, was placed on the top of pluviated sample and rubber membrane was then sealed to its outer surface. An Initial suction of 10 kPa was applied before removal of mold and sample's initial dimension was measured (as shown in Table 2). All samples were tested under dry condition.

Drained triaxial compression tests were conducted on dry samples under initial isotropic stress (applying through suction) of 25, 50 and 80 kPa, in a displacement controlled manner. The changes in radius of the sample were manually measured at three marked locations during shear wave velocity measurement (Fig. 3(d)) to compute its volume change.

Shear wave velocity was measured by a pair of bender elements installed at the top cap and pedestal (Lee and Santamarina 2005 and Teachavorasinskun and Amornwithayalax 2002). The double layer piezoceremic (brass reinforced) bender element with thickness of 0.51 mm was used as the generator and receiver of shear wave (Fig. 3). Both bender elements were inserted into the sample with protrusion of about 9.6 mm. A single excitation pulse of +10 DCV was first given to

Table 2 Initial conditions of tested samples

Sand type	Confining pressure (kPa)	Initial dry density (kN/m^3)	Initial void ratio	Final void ratio (measured)	Final void ratio (computed)
D16	25	14.09	0.908	0.997	1.146
	50	14.19	0.896	0.997	1.110
	80	13.97	0.925	1.015	1.129
	25	15.12	0.779	0.836	1.129
	50	14.94	0.799	0.868	1.038
	80	14.97	0.797	0.866	1.030
D40	25	13.39	1.031	1.121	1.221
	50	13.63	0.996	1.077	1.1362
	80	13.47	1.019	1.114	1.186
	25	14.53	0.873	0.935	1.119
	50	14.58	0.865	0.941	1.157
	80	14.58	0.865	0.931	1.169
Silica sand	25	16.76	0.581	0.654	0.776
	50	17.15	0.545	0.601	0.739
	80	16.91	0.568	0.651	0.774
	25	17.44	0.520	0.580	0.839
	50	17.77	0.491	0.554	0.670
	80	17.50	0.514	0.579	0.730

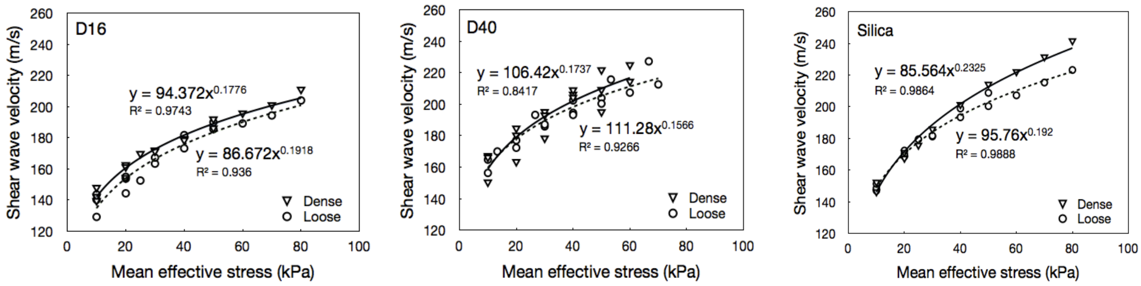

(a) D16 (b) D40 (c) Silica sand

Fig. 4 Shear wave velocity and mean effective stress during isotropic compression

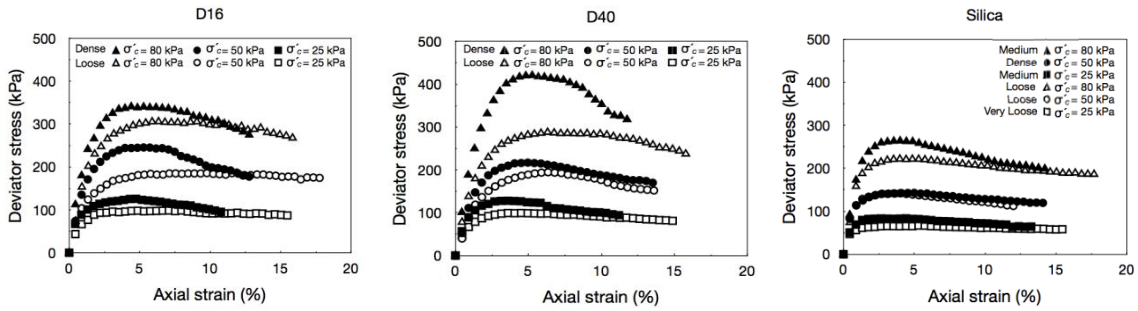

(a) D16 (b) D40 (c) Silica sand

Fig. 5 Deviator stress and strain relations during drained triaxial compression tests

the top bender element to generate a shear wave (Fig. 3(d)). It was then received by the pedestal bender element. In order to identify travel time, another single pulse of –10 DCV was excited. The travel time was determined from the first cross-polarization of those two received.

A commercially available sticker grid of 5×5 mm was carefully pressed and attached on the surface of rubber membrane (Fig. 3(a)) for taking digital images. However, the image was only used for reference not for detailed localization analysis, due to the lack of important information, e.g., relative stiffness of grid and membrane, membrane penetration, etc. Furthermore, due to usage of rough top and bottom platens, the observed localization in the tested sample was not accurate and was used for very preliminary examination only.

3. Results and discussion

Shear wave velocity, V_s, is governed by the states of effective stresses, which could be the mean effective stress (Teachavorasinskun and Amornwithayalax 2002, Teachavorasinskun *et al*. 2002 and Flores-Guzman *et al*. 2014) or those stress components in the wave motion plane (Roesler 1979, Yu and Richart 1984 and Ku and Mayne 2015). Fig. 4 shows the variations of shear wave velocity against mean effective stress obtained during isotropic compression. Since the stress state is isotropic, a simple correlation, as shown in Eq.(1), between shear wave velocity, V_s, and mean effective stress (confining stress), $p' = (\sigma_1' + 2\sigma_3')/3$, can be applied.

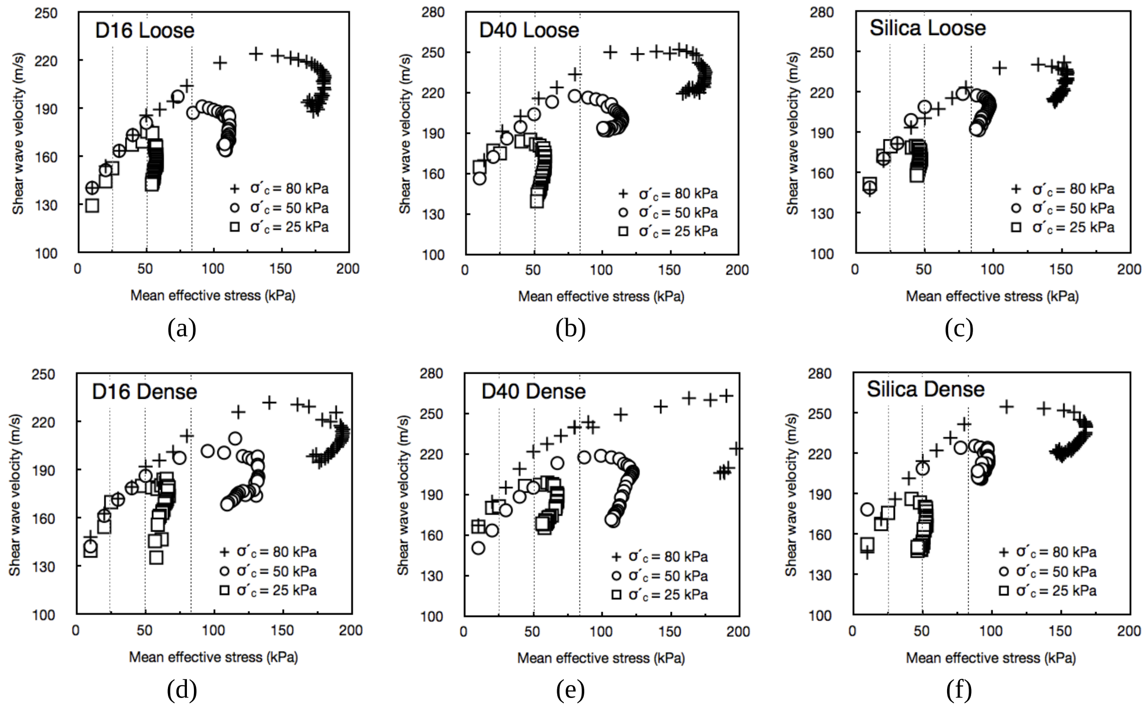

Fig. 6 Changes of shear wave velocity with respect to mean effective stress, *p'*, of loose and dense samples of D16, D40 and Silica sands during drained traixial compression

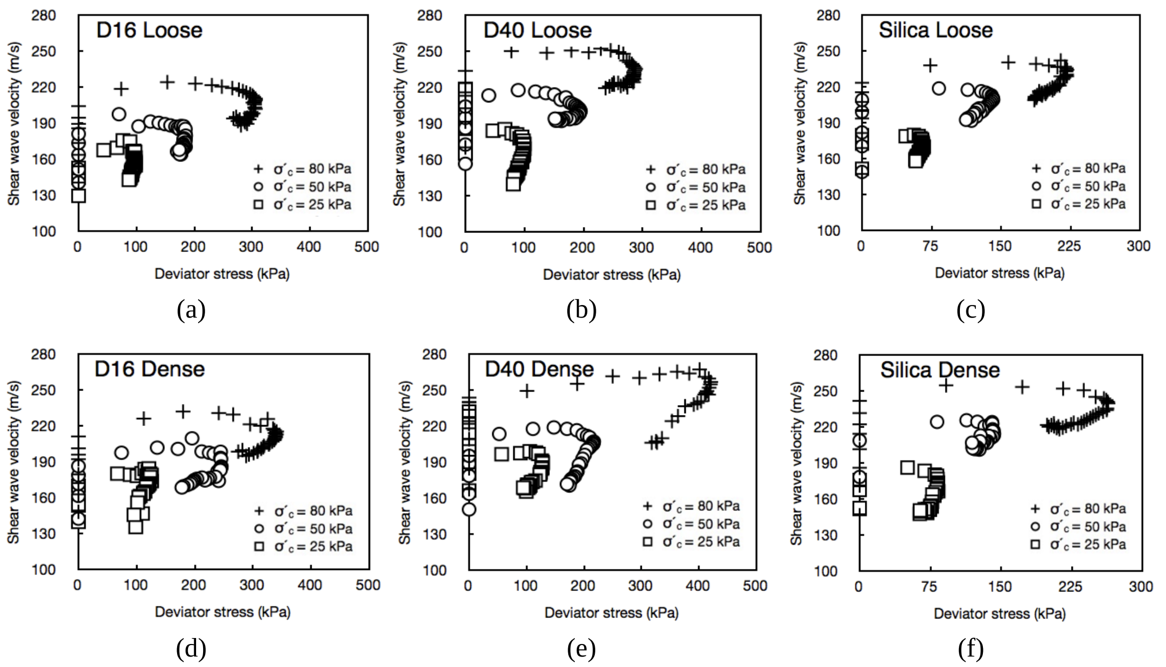

Fig. 7 Changes of shear wave velocity with respect to deviator stress, *q*, of loose and dense samples of D16, D40 and Silica sands during drained traixial compression

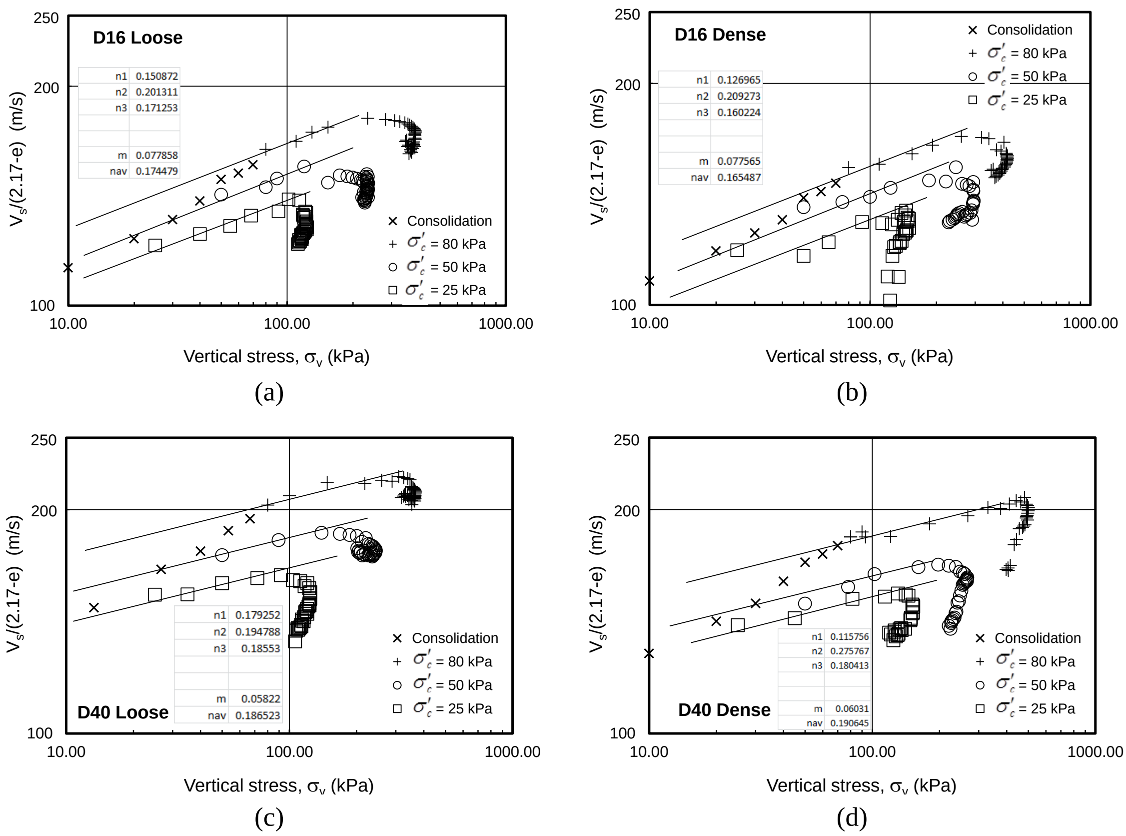

Fig. 8 Relationships between the vertical stress and shear wave velocity of D16 and D40 sands. Note that vertical gap between each line indicates influence of initial confining stress (parameter *n*)

$$V_s = K\left(\frac{\sigma_1^{'} + 2\sigma_3^{'}}{3}\right) \tag{1}$$

Where K is a parameter containing influence of void ratio, σ'_1 and σ'_3 are the vertical and confining stresses and R is a constant. Based on the results shown in Fig. 4, K of 85 – 100 and R of 0.16 – 0.23 are obtained from the tested sands, where the units of V_s and stresses are m/s and kPa, respectively.

The relationships between the deviator stress, $q = \sigma'_1 - \sigma'_3$, and vertical strain, ε_1, during drained compression are summarized in Fig. 5. The friction angles, ϕ = arcsin $\sigma'_1 - \sigma'_3)/(\sigma'_1 + \sigma'_3)]_{peak}$, vary in range of 42-44° for dense specimens and 39 - 40° for loose specimens of D16 and D40 sands. While slightly smaller friction angles of 35-39° is observed for silica sand. For most samples, the peak deviator stress, by visual observation, occurs at the axial strain of about 3 to 5%.

The shear wave velocity, V_s, during drained triaxial compression, is plotted against mean effective stress, p', and deviator stress, q, in Figs. 6 and 7, respectively. Note that V_s obtained during consolidation is also plotted. It is clearly seen that none of those two stress parameters could reasonably represent shear wave velocity variations obtained during triaxial compression stage. Namely, Eq. (1) is not applicable after completion of isotropic compression.

Roesler (1979) and Escribano and Nash (2015) proposed that the stresses in the wave propagation and particle motion directions, σ'_{pd} and σ'_{pm}, are the two main stress components affecting the shear wave velocity of sandy soil. The stress acting orthogonal to the wave motion plane can be neglected as shown in Eq. (2)

$$G = K_1 \cdot f(e) \cdot \sigma_{pd}{'}^{2m} \sigma_{pm}{'}^{2n} \tag{2}$$

Where m and n are material constants. Such correlations have been widely adopted in recent researches (Roesler 1979, Yu and Richart 1984, Cha *et al*. 2014 and Escribano and Nash 2015). In drained triaxial test and shear wave pattern adopted in the present study, $\sigma'_{pd} = \sigma'_1$ and $\sigma'_{pm} = \sigma'_3$ = constant. Since range of void ratio used in the present study is not sufficient to propose any void ratio function, the existing empirical equation, $f(e) = (2.17 - e)^2 / (1+e)$ (e.g., Iwasaki *et al*. 1978), is adopted. Substituting $G = \rho V_s^2$ and $\rho = \rho_d = G_s\rho_w / (1 + e)$, Eq. (2) can be written in term of V_s as

$$V_s = K_2 \cdot \frac{(2.17 - e)}{\sqrt{G_s \rho_w}} \cdot \sigma_1{'}^{m} \sigma_3{'}^{n} \tag{3}$$

or

$$\log\left(\frac{V_s}{2.17 - e}\right) = \log\left(\frac{K_2}{\sqrt{G_s \rho_w}}\right) + n\log(\sigma_3{'}) + m\log(\sigma_1{'}) \tag{4}$$

Where ρ_d = dry density of sample, ρ_w = density of water and G_s = specific gravity of sand. Since σ'_3 is constant for each test, the plot between the normalized shear wave velocity, $V_s / (2.17 - e)$, and vertical stress, σ'_1, on the logarithmic plot should be linear. The constant m is determined from the slope of the best fitted lines, which being practically parallel to each other as exhibited in Fig. 8. In drained triaxial compression test, the vertical stress can therefore provide better representation of shear wave velocity variation. The constant n is estimated from the vertical gap between pairs of solid lines obtained from tests with different confining pressures. Based on Eq.(4), three values of n can be obtained from each figure, namely, $n1$, $n2$ and $n3$ (as their values shown in the figures) are computed from two tests with confining stresses between 50 and 25 kPa, 80 and 50 kPa and 80 and 25 kPa, respectively. Variation of n computed from each pairs of tests is considered small.

However, as can be noted from Fig.8, after peak deviator stress was achieved, the normalized shear wave velocity, $V_s / (2.17 - e)$, reduced and deviated from the pre-peak trend lines. Localization is probably its main cause. Nevertheless, the un-normalized post peak shear wave velocity shown in Fig. 9 can partly due to the post-peak decrease of effective stress. The typical plots between post-peak shear wave velocity and vertical strain as shown in Figs. 9 and 10 give a better view for such post-peak reduction of V_s. In general, the decrease of shear wave velocity at post peak can be divided into two stages.

(1) The shear wave velocity decreases almost linearly with the increase in the vertical strain. This stage might govern the formation of narrow shear band and its expansion.

(2) In the second stage which occurred at higher strain after shear band formation, the rate of reduction became much smaller. The sample in this stage might internally re-arrange its overall density to approach a new stage of more uniform void ratio across the sample.

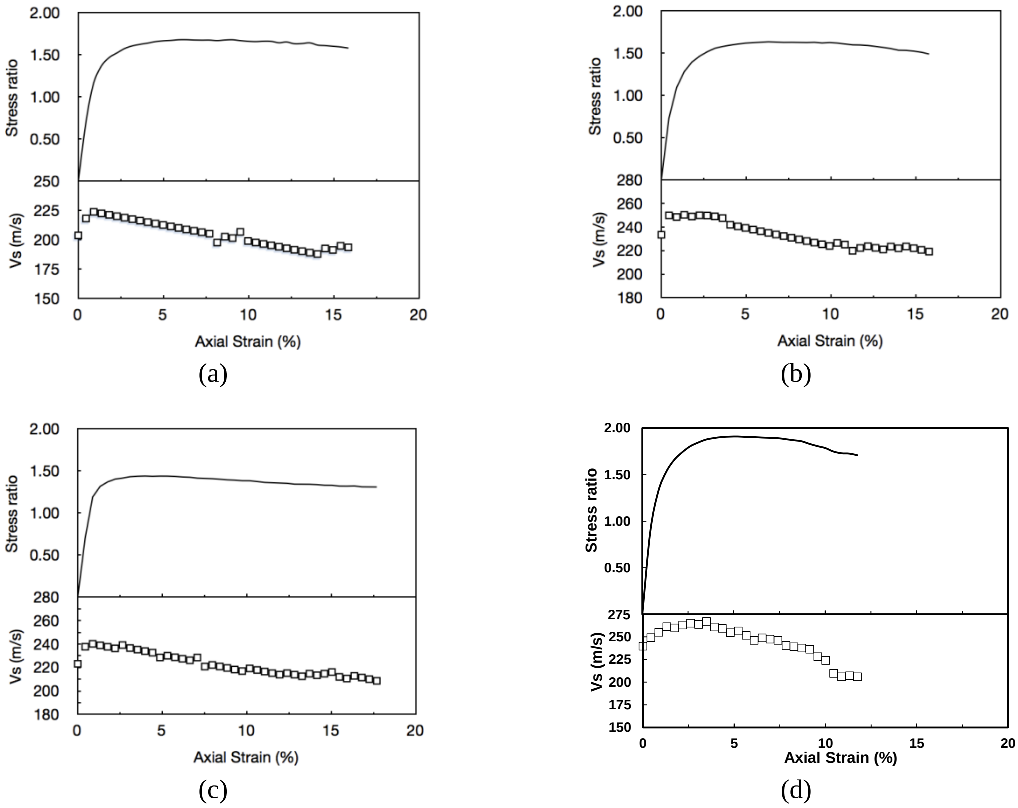

Fig. 9 Typical test results expressing the variation of post peak V_s versus axial strain

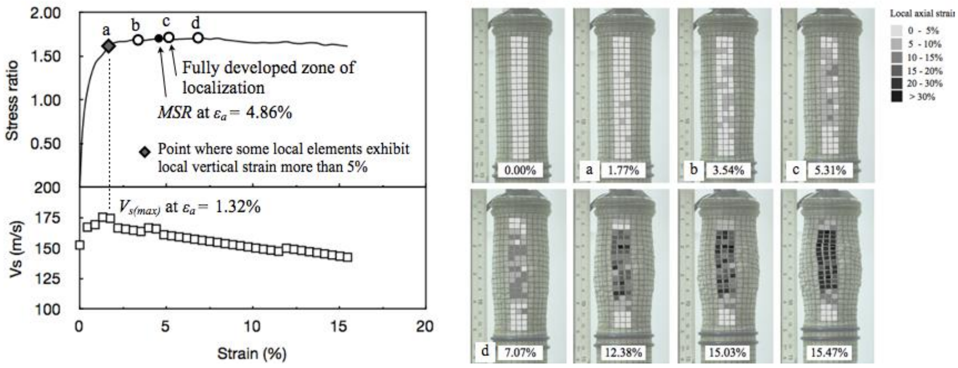

Fig. 10 Rough local strain profile during triaxial compression test of a loose D16 sample ($\sigma_c' = 25$ kPa)

A rough local strain profile estimated from the digital images (Fig. 10) can be used to support the above implication. After peak stress, large local strains were concentrated around the center of the sample. However, at very final stage of testing where strain was very large, almost uniform local strain could be observed. By adopting that, at the very final stage of testing, sample may re-arrange itself to the stage of almost uniform density and Eq. (3) is still applicable. Then the ratio of shear wave velocity at peak stress, $(V_s)_p$, and at final stage of testing, $(V_s)_f$, can be written as

$$\frac{(V_s)_p}{(V_s)_f} = \frac{(2.17 - e_p)}{(2.17 - e_f)} \cdot \left(\frac{(\sigma_1')_p}{(\sigma_1')_f} \right)^m \tag{5}$$

Where e_p and e_f and $(\sigma'_1)_p$ and $(\sigma'_1)_f$ are void ratios and vertical stresses at peak and at final stage of testing, respectively. Based on this equation, void ratios at final stage of each test, e_f, are computed and their values are summarized in Table 2. The values of e_f computed from each test are larger than the final void ratio computed from external measurement and are close to the corresponding maximum void ratios, $e_{\max}$.

4. Conclusions

The measurement of shear wave velocity along the whole path of drained triaxial compression test revealed that shear wave velocity during each state of testing formed various dependencies to stress and strain states. During isotropic compression, a widely recognized correlation between shear wave velocity and mean effective stress can properly express its stress dependency characteristics. During drained triaxial compression stage, a function governing individual stress parameters in the wave propagation plane was required. After peak deviator stress was attained, the shear wave velocity deviated from the previously existed tend line and reduced almost linearly with axial strain. This might be due to non-uniformity caused by the formation of shear band. However, at very large strain, sample may internally re-arrange itself to a more uniform loose stage. This final void ratio computed based on amount of reduction in shear wave velocity was found to be close to the value of the maximum void ratio.

Acknowledgments

The research presented herein was financially support by the Thailand Research Fund (TRF: RMU5180052), the Commission on Higher Education, Ministry of Education under Faculty Development Scholarship Program with the collaboration of AUN/SEED-Net and the Rachadaphiseksomphot Endowment Fund, part of the “Strengthen Chulalongkorn University Researcher’s Project”.

References

Bellotti, R., Jamiolkowski, M., Lo Presti, D.C.F. and O’Neill, D.A. (1996), “Anisotropy of small strain stiffness in Ticino sand”, *Géotechnique*, **46**(1), 115-131.

Cha, M.S., Santamarina, J.C., Kim, H.S. and Cho, G.C. (2014), “Small-strain stiffness, shear-wave velocity, and soil compressibility”, *J. Geotech. Geoenviron. Eng.*, **140**(10), 06014011.

Clayton, C.R.I. (2011), “Stiffness at small strain: Research and practice”, *Geotechnique*, **61**(1), 5-37.

Desrues, J. and Viggiani, G. (2004), “Strain localization in sand: an overview of the experimental results obtained in Grenoble using stereophotogrammetry”, *Int. J. Numer. Anal. Method. Geomech.*, **28**(4), 279-321.

Escribano, D.E. and Nash, D.F.T. (2015), “Changing anisotropy of G_0 in Hostun sand during drained monotonic and cyclic loading", *Soil. Found.*, **55**(5), 974-984.

Flores-Guzman, M., Ovando-Shelley, E. and Valle-Molina, C. (2014), "Small strain dynamic characterization of clayey soil from Texcoco Lake, Mexico", *Soil Dyn. Earthq. Eng.*, **63**, 1-7.

Hardin, B.O. and Drnevich, V.P. (1972), "Shear modulus and damping in soils: measurements and parameter effects", *J. Soil Mech. Found. Div.*, **98**(6), 603-624.

Higo, Y., Oka, F., Sato, T., Matsushima, Y. and Kimoto, S. (2013), "Investigation of localized deformation in partially saturated sand under triaxial compression using microfocus X-ray CT with digital image correlation", *Soil. Found.*, **53**(2), 181-198.

Iwasaki, T., Tatsuoka, F. and Takagi, Y. (1978), "Shear moduli of sands under cyclic torsional shear loading", *Soil. Found.*, **18**(1), 39-56.

Ku, T. and Mayne, P.W. (2015), "In situ lateral stress coefficient (K-0) from shear wave velocity measurements in soils", *J. Geotech. Geoenviron. Eng.*, **141**(12), UNSP 06015009.

Lee, J.S. and Santamarina, J.C. (2005), "Bender elements: Performance and signal interpretation", *J. Geotech. Geoenviron. Eng.*, **131**(9), 1063-1070.

Roesler, S.K. (1979), "Anisotropic shear modulus due to stress anisotropy", *J. Soil Mech. Found. Div.*, **105**(7), 871-880.

Silvestri, V. and Abou-Samra, G. (2009), "Analytical soulution of stress-strain relationship of modified Cam clay in undrained shear", *Geomech. Eng., Int. J.*, **1**(4), 263-274.

Stokoe, K.H. II, Hwang, S.K., Lee, J.N.K. and Andrus, R.D. (1995), "Effects of various parameters on the stiffness and damping of soils at small to medium strains", (Shibuya et al. Eds.), *Proceedings of the International Symposium on Pre-failure Deformation of Geomaterials*, (Volume 2), Sapporo, Japan, September, pp. 785-816.

Teachavorasinskun, S. and Akkarakun, T. (2004), "Paths of elastic shear modulus of clays", *Géotechnique*, **54**(5), 331-333.

Teachavorasinskun, S. and Amornwithayalax, T. (2002), "Elastic shear modulus of Bangkok clay during undrained triaxial compression", *Géotechnique*, **52**(7), 537-540.

Teachavorasinskun, S., Thongchim, P. and Lukkunaprasit, P. (2002), "Shear modulus and damping of soft Bangkok clays", *Can. Geotech. J.*, **39**(5), 1201-1208.

Xu, X.M., Ling, D.S., Cheng, X.P. and Chen, Y.M. (2015), "Correlation between liquefaction resistance and shear wave velocity of granular soils: A micromechanical perspective", *Geotechnique*, **65**(5), 337-348.

Yu, P. and Richart, F.E. (1984), "Stress ratio effects on shear modulus of dry sands", *ASCE J. Geotech. Eng.*, **110**(3), 331-345.

CC